

Differential remineralization of major and trace elements in sinking diatoms

Benjamin S. Twining,^{1,*} Scott D. Nodder,² Andrew L. King,^{3,a} David A. Hutchins,³
Gary R. LeClerc,⁴ Jennifer M. DeBruyn,⁵ Elizabeth W. Maas,² Stefan Vogt,⁶
Steven W. Wilhelm,⁴ and Philip W. Boyd^{2,7,b}

¹Bigelow Laboratory for Ocean Sciences, East Boothbay, Maine

²National Institute of Water and Atmospheric Research (NIWA) Ltd, Wellington, New Zealand

³Marine Environmental Biology, Department of Biological Sciences, University of Southern California, Los Angeles, California

⁴Department of Microbiology and The Center for Environmental Biotechnology, The University of Tennessee, Knoxville, Tennessee

⁵Department of Biosystems Engineering and Soil Science, The University of Tennessee, Knoxville, Tennessee

⁶X-ray Science Division, Advanced Photon Source, Argonne National Laboratory, Argonne, Illinois

⁷NIWA Centre of Chemical and Physical Oceanography, University of Otago, Dunedin, New Zealand

Abstract

Macronutrients in sinking phytoplankton are typically remineralized at different rates, but less is known about the fate of micronutrient metals associated with sinking cells. Scavenging, the presence of co-occurring abiotic particles, and inadvertent contamination limit the utility of bulk analytical approaches to study remineralization of trace metals in sinking phytoplankton. We used synchrotron x-ray fluorescence mapping to measure macronutrients (P, S, and Si) and trace metals (Fe, Ni, and Zn) in individual cells of the diatom *Asterionellopsis glacialis* during a spring bloom in subtropical waters off New Zealand. P, S, Zn, and Ni were released significantly faster than Fe and Si from sinking cells in the upper 200 m. Bulk particulate element fluxes to sediment traps indicated similar trends, but biogenic silica flux was attenuated much faster than Si was lost from intact sinking cells collected in the traps. The metals were spatially co-located with P and S in upper ocean cells, but this association with P and S (based on a spatial resolution of 450 nm) was largely absent in sinking cells. In contrast, Fe retained a weak spatial association with Si, suggesting that remineralized Fe may be re-scavenged onto cell surfaces. As a result, dissolved Fe:macronutrient stoichiometries in the water column likely underestimate stoichiometries in sinking cells. We propose linkages between the selective loss of diatom cellular components (e.g., ribosomes or phospholipid membranes, Zn-finger proteins, and urease) and the observed recycling of specific elements (P, Zn, and Ni, respectively), which set the stoichiometry of macro- and micronutrient supply to surface waters.

The growth and subsequent sinking of phytoplankton-derived biogenic particles mediates the downward vertical flux of C and other nutrient elements from the surface ocean. This ‘biological pump’ removes C from the upper ocean–atmosphere system and hence plays an important role in Earth’s climate system. Sinking biogenic particles are degraded by microbial and zooplanktonic activities (Steinberg et al. 2008) and are also altered by abiotic dissolution and scavenging processes. The net effect of these processes at depth is remineralization, which we define here as the breakdown of biogenic particles, including microbially mediated enzymatic solubilization. Deep waters then resupply these released nutrients to surface waters by processes such as advective upwelling, convective overturning, and deep winter mixing. Critically, the depths at which elements are remineralized affects the rates of their subsequent return to the surface; and changes in the depths over which elements are remineralized can

thus indirectly influence atmospheric CO₂ concentrations over periods of decades to centuries (Kwon et al. 2009).

Elements are remineralized from sinking cells through several mechanisms. Laboratory experiments with decomposing phytoplankton indicate that remineralization is often microbially mediated (Lee and Fisher 1992; Bidle and Azam 1999), and thus remineralization is affected by in situ temperature and the composition of both particles and microbial communities. Individual cells or aggregates may also be consumed by mesozooplankton and associated elements returned to the dissolved phase via sloppy feeding, zooplankton excretion, or viral lysis. Sinking cells and aggregates are also prone to microbial degradation and subsequent dissolution (Karl et al. 1988). Released elements diffuse into the water column after enzymatic attack or are scavenged onto particle surfaces, as seen with some metals (Lee and Fisher 1993; Frew et al. 2006). Further, the fate of different types of particles, and their building blocks, will be determined by their differential labilities. Dense fecal pellets and larger ballasted phytoplankton aggregates may sink rapidly and remove elements to deeper depths prior to remineralization, while individual cells and less consolidated aggregates may be prone to microbial degradation and recycling in shallow waters. Information about the fate of elements in specific particle types is needed for the accurate modeling of these processes,

* Corresponding author: btwining@bigelow.org

Present address:

^aNational Oceanic and Atmospheric Administration, Northeast Fisheries Science Center, Milford, Connecticut

^bInstitute for Marine and Antarctic Studies, University of Tasmania, Hobart, Tasmania, Australia

including quantitative estimation of the effect of microbial community and grazer composition on particle export and remineralization.

Major bio-elements are known to be remineralized from sinking plankton at different rates. Dissolved nutrient profiles typically show N and P to be remineralized at shallower depths than Si (Broecker and Peng 1982), and N and P are often released more rapidly than C (Shaffer et al. 1999; Brea et al. 2004). Measurements of sinking particle fluxes in sediment traps also show decoupling of C, N, and P remineralization, with P and N lost before C (Schneider et al. 2003). In some instances, P is also remineralized before N (Loh and Bauer 2000). Together, these studies reveal a generalized gradient of remineralization length-scales of $P \leq N < C < Si$ (Boyd and Trull 2007).

Less is known about the relative remineralization rates of trace-metal micronutrients from sinking cells. Several issues present challenges to this research. Trace metals occur at much lower concentrations in the ocean than macronutrients, and metals are more prone to inadvertent contamination during sampling and analysis. Thus, relatively few studies have attempted the logistically difficult task of sampling vertical fluxes of trace elements using 'clean' techniques and procedural blanks (Frew et al. 2006). Additionally, abiotic processes such as authigenic mineral formation and adsorptive scavenging are important for metals such as Mn, Fe, and Co (Chester 2003; Noble et al. 2012), and these processes may mask biological remineralization processes in the water column. Further, particles of lithogenic and authigenic origin are often a significant component of particulate metal pools (Frew et al. 2006; Lamborg et al. 2008; Barrett et al. 2012), confounding interpretations of biogenic particle behavior from bulk geochemical measurements. Although there is some evidence for decoupled remineralization of biogenic trace metals (Lamborg et al. 2008; Boyd and Ellwood 2010), in many instances it is not known whether remineralization of biogenic trace metals is coupled to that of major elements. It is also not known to what extent differences in metal remineralization are due to differences in the behaviors of the various particle types (i.e., biogenic vs. lithogenic) compared with differences in the behaviors of the metals within a given particle type. Critically, the heterogeneous nature of sinking particle assemblages collected in sediment traps precludes studying the behavior of individual functional groups with traditional bulk analytical approaches.

Here we use single-cell synchrotron x-ray fluorescence (SXRF) analysis to analyze individual components of sinking material collected using trace-metal-clean techniques during a spring bloom in the ocean. With this approach, we are able to focus analyses on a single taxon of sinking diatoms that was the dominant species of the phytoplankton bloom. We report direct evidence of differential remineralization of bioactive elements—comprising both major and trace elements—measured in suspended and sinking diatoms during a bloom event. These results suggest that autolysis and/or microbial degradation, likely followed by selective scavenging, results in decoupled remineralization of different elements in the water column.

Methods

Sample collection—Samples were collected as part of the FeCycle II GEOTRACES process study of trace-metal biogeochemistry during the annual spring diatom bloom in subtropical waters 280 km east of the North Island, New Zealand (Boyd et al. 2012). Waters were sampled within an anticyclonic eddy centered on 39°20'S 178°40'W using a quasi-Lagrangian approach with drogued drifter buoys. All stations were within 25 km of this location. Cells of the centric diatom species *Asterionellopsis glacialis*, as well as bulk particles $> 0.2 \mu\text{m}$, were collected from 30 m and 60 m using Teflon-coated Niskin-X bottles deployed on a trace-metal-clean rosette. Samples for size-fractionated chlorophyll were taken from 5, 30, 60, 100, and 200 m on the same casts. Sinking cells and particles were collected at 100 m and 200 m using trace-metal-clean free-drifting, cylindrical MULTI-sediment traps (7 cm diameter; aspect ratio, height:diameter = 8.3 [Martin et al. 1987; Frew et al. 2006]). Sediment traps were deployed for 72 h on four separate occasions. The second deployment (A2) occurred from day of the year (DOY) 267–270—corresponding to the *A. glacialis* bloom—and synchrotron and bulk data correspond to this deployment.

Bulk sediment-trap particles were collected in baffled cylinders back-filled with Chelexed brine solution poisoned with $< 1\%$ trace metal-cleaned chloroform (Frew et al. 2006). Procedural blanks consisting of sealed tubes were included in each deployment and confirmed low levels of metal contamination. All traps were screened for zooplankton 'swimmers' $> 200 \mu\text{m}$ prior to sampling. Bulk particulate N fluxes were determined in samples filtered onto pre-combusted HCl-washed GF/F membranes using a modified Kjeldahl method (Downes 1978). Bulk biogenic silica fluxes were determined by NaOH digestion of trap material collected on pre-weighed 25 mm diameter 0.2 μm pore-size polycarbonate membrane filters (Ragueneau and Tréguer 1994). Particulate material for inductively coupled plasma mass spectrometry (ICPMS) analysis was immediately filtered onto acid-washed 47 mm diameter 0.2 μm pore-size polycarbonate membrane filters and rinsed with an oxalate and ethylenediaminetetraacetic acid solution (mixed-layer samples) or 0.2 μm filtered seawater (trap samples). The oxalate solution was not used on trap samples because of uncertainty about the effect of this rinse on potentially degraded sinking cells, because development and testing of the rinse was previously performed with healthy, intact phytoplankton (Tovar-Sanchez et al. 2003). Based on preliminary data, this difference in rinse treatment may result in $\sim 40\%$ lower particulate Fe concentrations in the mixed-layer compared with trap samples (see further discussion below). All ICPMS samples were stored frozen at -20°C until analysis. Cells for synchrotron analysis were collected from unpoisoned traps and were immediately preserved with 0.25% trace-metal-clean glutaraldehyde prior to centrifugation onto transmission electron microscopy grids using clean techniques following the protocols of Twining et al. (2003).

SXRF analyses—Individual *A. glacialis* cells were analyzed by SXRF microprobe, providing quantitative measures of element quotas and two-dimensional maps of

element distribution within each cell (Twining et al. 2003). Cells were analyzed at beamline 2-ID-E of the Advanced Photon Source, Argonne National Laboratory. Twenty-six individual cells were analyzed in total, including 14 collected from the surface mixed-layer and 7 and 5 cells from the 100 m and 200 m traps, respectively. Each cell was raster-scanned with a focused 10 keV x-ray beam with a diameter of $\sim 0.45 \mu\text{m}$. Step sizes were $0.4 \mu\text{m}$ and dwell time at each pixel was typically 1 s. Fluorescence spectra from the pixels covering the cell were averaged to calculate whole-cell quotas, and a fluorescence spectrum from a neighboring empty section of the grid was subtracted. Cellular K_{α} fluorescence intensities for Si, P, S, Fe, Ni, and Zn were then fit with a modified-Gaussian model using custom software and peak areas converted to areal element concentrations using National Bureau of Standards certified standard reference materials (Twining et al. 2011).

Carbon and N cannot be detected in the cells via SXRF because of low fluorescence yields, small photo-electric absorption of the incident 10 keV beam, and significant fluorescence self-absorption for these elements. Sulfur is readily detectable and has been used as an alternate proxy for cell biomass in previous SXRF studies (Twining et al. 2004, 2011). Sulfur associated with dimethylsulfoniopropionate is likely lost from cells prepared for SXRF by fixation with glutaraldehyde. Therefore the dominant forms of cellular S detected with SXRF are likely to be cysteine and methionine amino acids incorporated into proteins. Proteins are also the major reservoir of N in phytoplankton (Sterner and Elser 2002). Although the S content of proteins can vary in response to environmental factors (Bragg et al. 2006), this would change the stoichiometry but not the qualitative analogous behavior of S and N. Sulfur may also be incorporated into sulfolipids in diatoms, but these are likely to be only a minor component of lipid membranes under the P-replete conditions observed during FeCycle II (Boyd et al. 2012). Thus, S serves as an alternative proxy for organic matter in phytoplankton that is expected to mimic N more closely than P.

Element attenuation coefficients were calculated for *A. glacialis* cells collected from the various selected depths. Mean element quotas for cells collected from 60 m were not significantly different (Wilcoxon test, $p > 0.05$) from those of cells from 30 m for any of the elements, and all suspended cells were grouped together for calculation of attenuation coefficients. Attenuation coefficients were calculated by fitting to the data the power law equation: $\text{quota} = a (\text{Depth})^{-b}$, where a and b are constants and Depth is in meters (Martin et al. 1987; Lutz et al. 2007).

Element co-localization within cells was investigated by plotting pixel-specific areal concentrations ($\mu\text{g cm}^{-2}$) of one element against those of another element in the same pixel; only pixels representing the cell in the two-dimensional scan were included in the analysis. Linear regressions of pixel-specific concentrations were used to assess changes in sub-cellular element spatial correlations with depth. The calculated coefficients of determination (r^2) for each element pair were averaged over all cells sampled from a given depth, and a Kruskal–Wallis test (JMP

version 7; SAS Institute) was used to test for significant changes in the mean coefficients of determination with depth. Depth changes in *relative* spatial correlations between element pairs in individual cells were also examined. In this case, we took advantage of the single-cell nature of the data set and performed pair-wise comparisons of spatial associations within each cell. For example, the spatial association (i.e., coefficient of determination, r^2) of Fe and P within cell No. 1 was compared with the association of Fe and Si within cell No. 1. This was repeated for all cells at the same depth, and the data for each depth were then grouped and tested for statistically significant differences in the coefficients of determination of the two element pairs using a Wilcoxon Signed Rank Sum Test.

Bulk element ICPMS analyses—Particulate samples for ICPMS trace-metal and P analysis were thawed and processed in a trace-metal-clean laboratory using a complete acid digestion protocol (Eggemann and Betzer 1976) as described by King et al. (2012). Sample and blank filters were placed in digestion bottles and refluxed in 750 μL ultrapure HCl for 30 min in a 100°C water bath, then 250 μL ultrapure HNO₃ was added and refluxed for an additional 30 min, then finally 50 μL ultrapure HF was added and refluxed for 1 h. Samples were cooled for ≥ 30 min between acid additions and all work was performed in a HEPA-filtered laminar-flow fume hood to minimize contamination. The final digest solution was diluted (1:5 v:v) using ultrapure water and transferred (with filter remnants) to acid-washed 15 mL low-density polyethylene bottles.

Elements were quantified with a magnetic sector high resolution inductively-coupled plasma mass spectrometer (Element 2; Thermo). The ICPMS was calibrated using a multi-element standard and calibration checked with the certified reference material SLRS-4 (National Research Council, Canada; recovery ranged 94–109%). Prior to analysis, 150 μL particulate sample digest was added to 850 μL 5% ultrapure HNO₃ spiked with a 1 $\mu\text{g} : \text{kg}$ ¹¹⁵In internal standard. Samples were introduced via an auto-sampler attached to a Teflon nebulizer (PFA-ST nebulizer; Elemental Scientific) coupled with a PC³ cyclonic spray chamber (Elemental Scientific). The ICPMS was tuned daily using a 1 $\mu\text{g} : \text{kg}$ ¹¹⁵In solution and mass offsets were corrected with a 5 $\mu\text{g} : \text{kg}$ multi-element standard. Procedural filter blanks were also subjected to the same storage, digestion, dilution, and analysis processes, and these blank values were subtracted from values for sample measurements.

Photoautotroph quantification and classification—Concentrations of phytoplankton in the water column were quantified in several ways. Size-fractionated Chlorophyll *a* (Chl *a*) concentrations were determined for microphytoplankton ($> 20 \mu\text{m}$) by passing samples through 47 mm diameter polycarbonate filters (GE Osmonics). Chl *a* was extracted from the filters in 90% acetone at 4°C overnight. Concentrations were quantified using a 10-AU fluorometer (Turner Designs) using the non-acidification protocol (Welschmeyer 1994). *A. glacialis* cells were directly counted

in surface waters (5 m) using manual microscope counts of Lugol's-preserved phytoplankton. To complement these data and place them within the context of the whole phytoplankton community, the relative abundance of photoautotrophs deeper in the water column (100 m) was assessed at different time points using PCR and high-throughput pyrosequencing of 16S rDNA sequences. DNA was extracted from particles in water samples collected onto 0.2 μm polycarbonate filters using the MoBio ultraclean soil DNA kit (MoBio). Fragments of 16S rRNA genes (~ 580 base pairs, encoding the hyper-variable V3–V5 regions) were amplified using primers 338F and 926R (Wang and Qian 2009) and Platinum Taq DNA polymerase (Invitrogen). After the initial Polymerase Chain Reaction (PCR) amplification (30 cycles), PCR products were purified with the Qiaquick PCR cleanup kit (Qiagen). A second round of PCR (6 cycles) was performed on the individual PCR products to add 454 fusion primers and multiplex identifiers (MIDs) to each sequence (Hamady et al. 2008). Individual products were then pooled and once again cleaned up using the Qiaquick PCR cleanup kit. The pooled products were prepared for unidirectional pyrosequencing using 454 Titanium chemistries according to manufacturer's protocols (454 Life Sciences) at the University of Tennessee – Oak Ridge National Laboratory Joint Institute for Biological Sciences.

Sequences were processed and trimmed using the MOTHUR (version 1.19) software package. After preprocessing our sequences for sufficient quality (qaverage = 25) and length (minlength = 450); 7183 sequences remained. These 7183 sequences were then classified using the Ribosomal Database Project classifier within MOTHUR. Sequences for phototrophs, which include those related to the bacillariophyta, cryptomonadaceae, chlorophyta, chlorarachniophyceae, streptophyta, or cyanobacteria were analyzed further. The sum total of these sequences was considered as the 100% total for phototrophic community structure, with the contribution of each of the above groups then considered relative to the total phytoplankton community. These photoautotrophic sequences were organized by sample date. Total counts were normalized between sample dates and each phylogenetic lineage was then reported as the percentage of reads of photoautotrophic origin within each sample. Using these approaches, we determined the temporal change in *A. glacialis* and the large ($> 20 \mu\text{m}$) phytoplankton community, as well as the proportion of the phytoplankton community represented by *A. glacialis*.

Results

A full description of the hydrography and biogeochemical setting during FeCycle II is presented elsewhere (Boyd et al. 2012; Weller et al. 2013). The surface mixed-layer was initially > 60 m and shoaled rapidly to ~ 30 m on DOY 267 (Fig. 1B; Weller et al. 2013). Mixed-layer temperature was $\sim 13^\circ\text{C}$. Transmissivity, a proxy for particle abundances, revealed a phytoplankton bloom beginning on DOY 267 and continuing through DOY 270. Chl *a* abundance and transmissivity indicated the beginning of

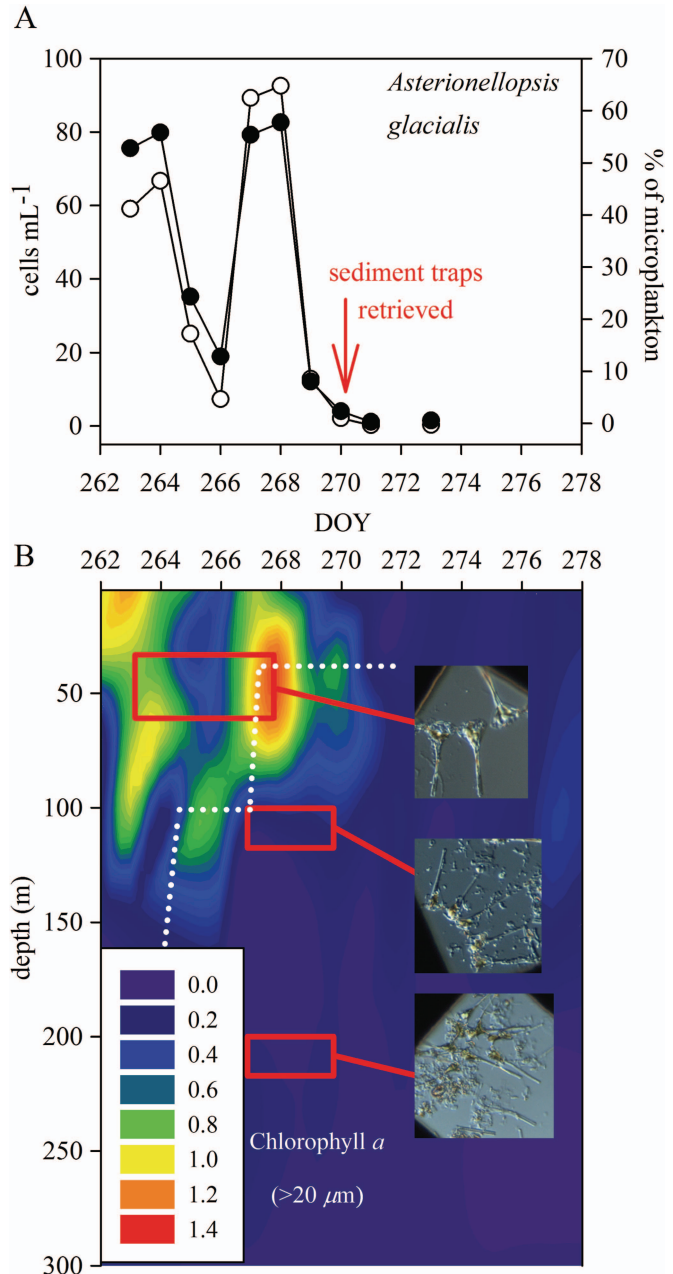


Fig. 1. (A) Concentration of *Asterionellopsis glacialis* cells (filled circles) and percentage of all nano- and microphytoplankton cell counts accounted for by *A. glacialis* (open circles) in the mixed-layer (5 m) over the course of the diatom bloom. (B) Subsurface concentrations ($\mu\text{g L}^{-1}$) of $> 20 \mu\text{m}$ Chl *a* as a function of time. The red boxes indicate the time and depth of cell collection for SXRF analysis. The dotted white line indicates the base of the mixed-layer. The surface layer cells were collected with Niskin-X bottles and the 100 m and 200 m cells were collected with free-drifting sediment traps deployed for 3 d. DOY—day of the year.

bloom decline at this point, immediately prior to a wind event on DOY 271–272, which ejected the drogued drifter buoy from the eddy (Boyd et al. 2012). A more complete presentation of the chlorophyll data is provided in Weller et al. (2013).

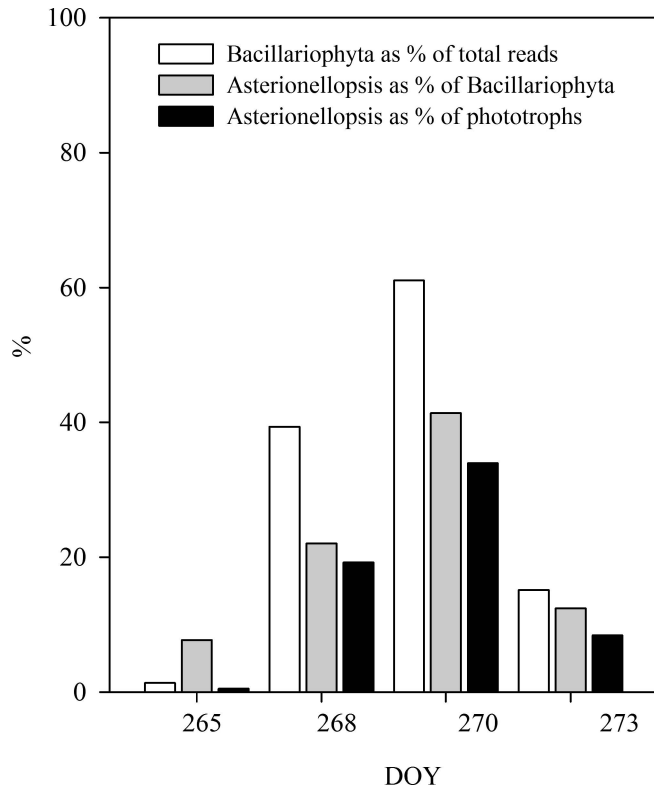


Fig. 2. Abundance of *Asterionellopsis* 16S rDNA sequences in samples collected at 100 m over the course of the diatom bloom. *Asterionellopsis* abundances are presented as a percentage of all diatom sequences (grey) and a percentage of all photoautotrophic sequences (black). The abundance of diatom sequences as a percent of total sequence reads is presented in white. A clear shift is evident from pre-bloom conditions (DOY 265) to the peak of the bloom export (DOY 270).

Both light microscopy and analysis of 16S rDNA sequences indicate that diatoms comprised a major component of the microplankton community during the bloom, with the araphid pennate diatom *A. glacialis* being the most abundant diatom (Figs. 1, 2). Concentrations of *A. glacialis* dropped rapidly over the course of several days, and by DOY 271 they were < 10% of the microplankton community. Sediment traps deployed to 100 m and 200 m depth from day 267 to day 270 captured abundant *A. glacialis* cells (Figs. 1, 3). Both individual cells and bulk particles were collected from the surface mixed-layer, and sinking cells and particles were intercepted by free-drifting sediment traps at 100 m and 200 m within 24 h of the bloom decline.

Element analyses of individual *A. glacialis* cells with SXRF demonstrate markedly differing rates of loss of both major biomass (P, S, and Si) and trace-metal (Fe, Ni, and Zn) constituents. Phosphorus and S were rapidly released from sinking cells, with mean (\pm standard error [SE]) P quotas decreasing from 51 ± 8 fmol cell⁻¹ in surface mixed-layer samples to 23 ± 8 and 17 ± 4 fmol cell⁻¹ at 100 m and 200 m, respectively (Fig. 4A). Cellular S dropped 75% from suspended cells to cells in the 100 m trap and an additional 32% by 200 m (Fig. 4B). Both

changes were statistically significant ($p < 0.05$; Table 1). In contrast, no consistent change in cellular Si was observed between the different depths ($p = 0.146$; Fig. 4C). Trace-metal remineralization was also decoupled, as cellular Zn and Ni quotas decreased by 76% and 61%, respectively, over the upper 200 m (Fig. 4E, F), compared with only a 25% decrease in Fe quotas (Fig. 4D). Of the metals, only the change in Zn was statistically significant ($p < 0.05$; Table 1).

Bulk fluxes measured in the sediment traps also show notable differences in element remineralization. These trends qualitatively match the relative trends seen in individual *A. glacialis*, with the exception of Si. Between 100 m and 200 m, bulk C and N fluxes decreased 45% and 55%, respectively, compared with a 32% decrease in cellular S. Bulk P flux decreased by 66%, and cellular P dropped by 28%. Nickel flux decreased $42\% \pm 38\%$, and bulk Zn flux decreased by $66\% \pm 31\%$ (Table 1). Bulk particulate Fe fluxes decreased only 4% between 100 m and 200 m. However, bulk biogenic Si fluxes decreased to the greatest extent (85%) between sediment traps at the two depths, in marked contrast to the Si quotas of *A. glacialis*, which did not significantly decrease. These data cannot be compared with surface values because fluxes were not measured in the mixed-layer. However, the flux data are internally consistent and not subject to differences in bulk particle rinses used in the surface and traps. The bulk flux data support the individual cell data in showing a decoupling of remineralization of both major elements and trace metals. Remineralization of bulk P and Si were both faster than loss of these elements from sinking cells captured at the same depths.

Normalization of bulk particulate metals to particulate P or Si enables comparisons of stoichiometries among all three collection depths. Phosphorus-normalized Fe and Ni stoichiometries were notably higher in bulk particles than in individual *A. glacialis* cells collected from the same depth, suggesting that significant amounts of Fe and Ni in the bulk pool were non-biogenic (Fig. 5). In contrast, bulk and cellular Zn:P were similar, indicating that particulate Zn was mostly biogenic. Bulk particles in the mixed-layer were treated with an oxalate rinse, which could have removed up to 40% of the Fe. If mixed-layer particulate Fe values were corrected for this potential 40% loss Fe:P would be 40% higher, providing even stronger support to the conclusion that much of the particulate Fe was lithogenic or at least non-biogenic. Data demonstrating the effect of oxalate rinsing on particulate Ni and Zn are not available, but a previous study shows that very little if any cellular Zn is removed by the oxalate wash (Tang and Morel 2006), so artifacts are expected to be smaller for Zn than for Fe.

Changes in bulk stoichiometries with depth qualitatively match changes in cellular stoichiometries. Bulk Fe:P increased \sim four-fold and cellular Fe:P increased \sim two-fold (Fig. 5). Correcting surface-bulk Fe for potential 40% removal via oxalate would result in a 2.6-fold increase in bulk Fe:P between the mixed-layer and 100 m. Only very minor changes in Zn:P were seen between the mixed-layer and 100 m, suggesting that these elements were remineralized

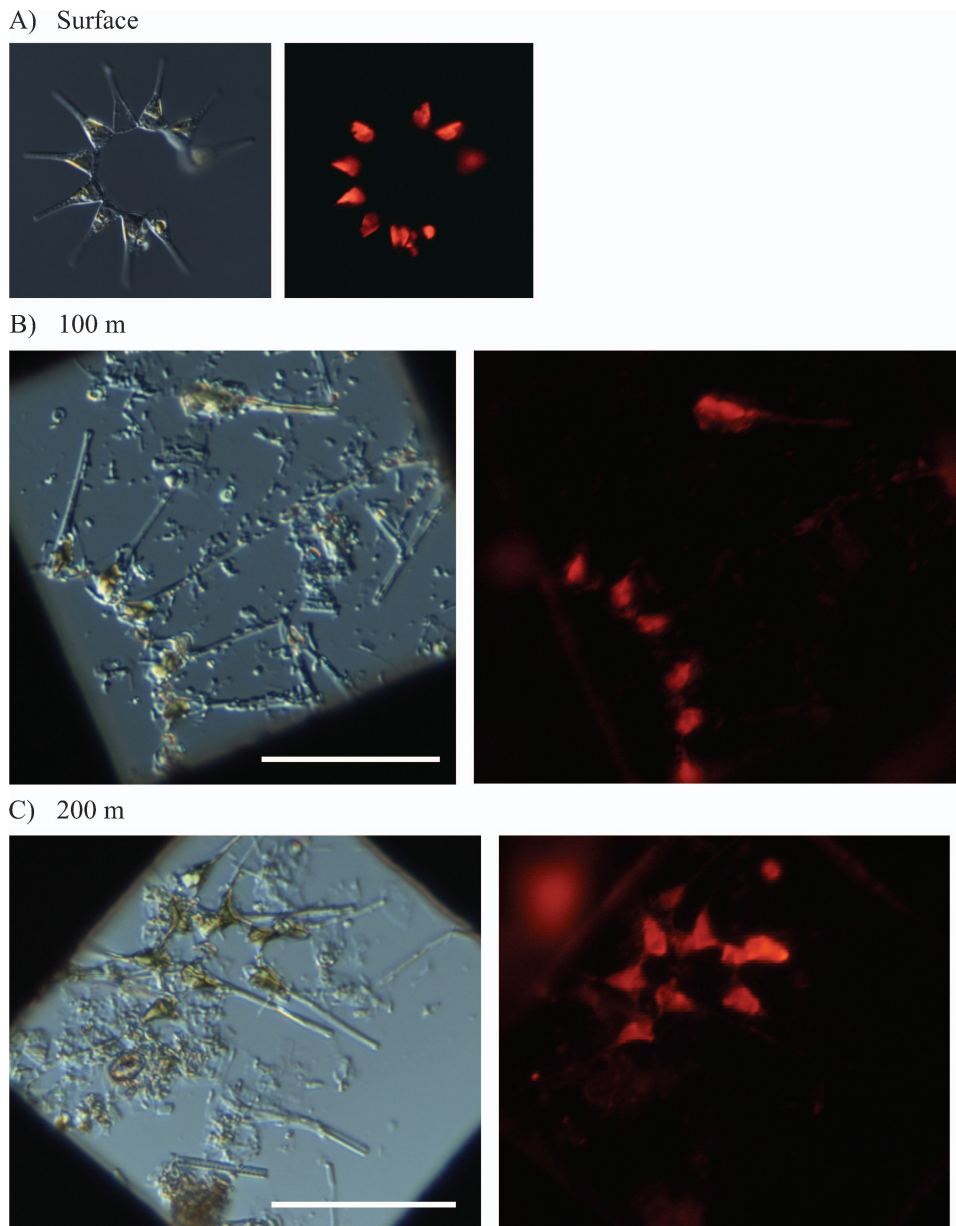


Fig. 3. Light (differential interference contrast) and epifluorescence (480 nm excitation) micrographs of *A. glacialis* cells collected from (A) the surface mixed-layer, (B) 100 m sediment trap, and (C) 200 m sediment trap. Chlorophyll fluorescence is evident in cells at each depth, strongly indicative of the presence of intact chloroplasts within cells. The scale bar indicates 40 μm .

together. Cellular Ni:P dropped 53% by 100 m, and bulk Ni:P dropped 76% by 100 m (Fig. 5). Although the magnitude of the changes are somewhat different, the similar direction of changes suggest that the remineralization processes acting on *A. glacialis* were occurring on other cells and particles as well.

The elemental stoichiometries of material lost from sinking cells provide insights into underlying remineralization mechanisms. These were calculated by dividing the difference in mean metal quotas of cells at the two depths of interest by the difference in mean biomass element (P, S, or Si) quotas of cells at the two depths. The Fe:P and Fe:S

stoichiometries of cellular components remineralized from diatoms in the upper 100 m (0.5 and 0.14 mmol:mol, respectively) were five- to seven-fold less than those measured for mixed-layer diatom cells (2.6 and 1.0 mmol:mol, respectively; Table 2). Thus, the biomolecules most readily solubilized by microbes from sinking cells—either passively or actively—appear to be largely non-Fe-containing moieties (e.g., nucleic acids and phospholipids). In contrast, Zn and Ni stoichiometries of components remineralized from diatoms in the upper 100 m were comparable to those of mixed-layer diatom cells, suggesting that Zn and Ni were lost as intact biomolecules (e.g.,

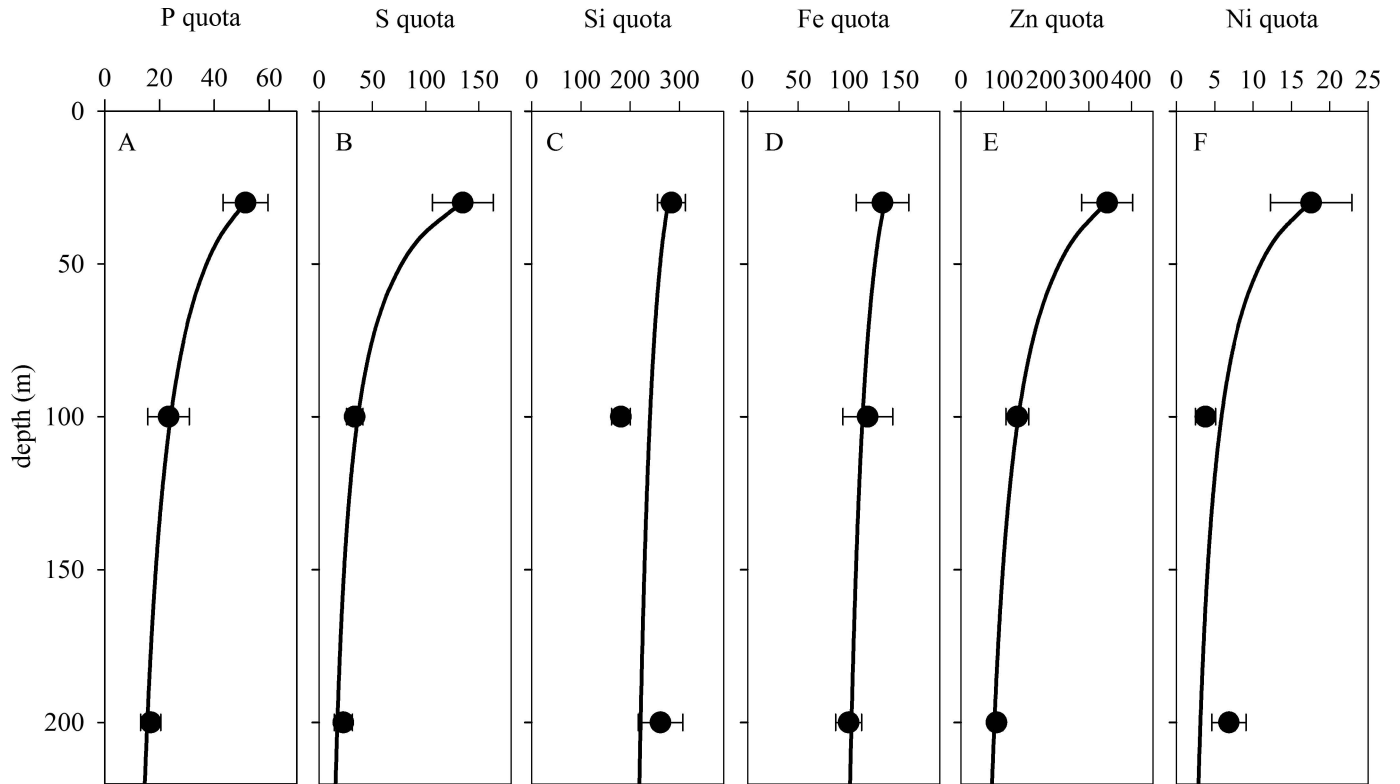


Fig. 4. Depth profiles of *Asterionellopsis glacialis* cellular element quotas for (A) P, (B) S, (C) Si, (D) Fe, (E) Zn, and (F) Ni. The quotas are means \pm SE ($n = 5-14$). A power-law function ($\text{Flux} = a(\text{depth})^{-b}$) has been fitted to each data set and the resulting attenuation coefficients (b) for the cells are shown in Table 1. P, S, and Si quotas are presented as fmol cell^{-1} , while Fe, Zn, and Ni quotas are presented as amol cell^{-1} .

proteins; Lee and Fisher 1993) or in conjunction with P and S moieties.

Additional information on sub-cellular biochemical associations and remineralization mechanisms is provided by analysis of the spatial distributions of the elements retained within cells. Correlations of elements within individual diatoms from different depths show that biogenic elements generally become less spatially correlated with each other as cells sink (Fig. 6). For example, cellular regions with higher Fe and S concentrations—indicating areas with organelles or other sub-cellular features enriched in these elements—tend to be spatially correlated in cells from the surface mixed-layer (Fig. 6B). In cells collected from sediment traps distributions of these elements have been altered by remineralization processes, and regions with high element concentrations are less likely to be spatially co-located (Fig. 6D). Comparisons of mean coefficients of determination (r^2) for element pairs at different depths demonstrate that, with the exception of Zn–S, metals became spatially decoupled from the biomass proxies P and S as cells sank (Table 3). However Fe maintained its weak spatial association with Si in the frustule even at 200 m, and Zn and S retained a strong spatial association (mean $r^2 = 0.48$) even at 200 m.

Pair-wise statistical comparisons of spatial associations of elements within each cell provide additional evidence of different behaviors of the three bioactive metals. Because the coefficients of variation are calculated for individual

cells, the relative correlation of the elements in each cell can be directly compared. For example, the correlation of Fe and P in a certain cell can be compared with the correlation of Fe and Si in the same cell. The relative magnitude of the coefficients of determination between element pairs in cells from each depth were then aggregated and tested for significant difference from no difference in spatial correlation between the element pairs using a non-parametric Wilcoxon Signed Rank Sum test. The statistical results are summarized in Table 4. Iron was equally associated with P and S at all 3 depths; Ni showed the same behavior. In contrast, Zn was significantly more associated with S than P at the surface and 100 m. This further supports a unique association between Zn and S. Iron was significantly more associated with P and S than with Si at the surface, but this association was lost at depths below 100 m for P and below 200 m for S, again suggesting movement of Fe from P and S moieties (e.g., protein) to Si moieties (e.g., frustule) or maintenance of Fe–Si associations while moieties with Fe, P and S were degraded. Contrasting this, Zn was more associated with S than with Si throughout the upper 200 m, although this difference was only weakly significant at 200 m ($p = 0.063$). Iron was somewhat more associated with Si than was Zn at all depths ($p < 0.08$). Nickel was significantly more associated with P (but not with S) than with Si in the upper 100 m, but this association was lost by 200 m depth, likely as a result of outer membrane degradation and loss of these elements from the cells.

Table 1. Remineralization of elements from sinking *Asterionellopsis glacialis* cells and the bulk particle assemblage. First three rows present mean (\pm SE) cell quotas for each depth. P, S, and Si are in units of fmol cell⁻¹, Fe, Zn, and Ni are in units of amol cell⁻¹. The letters following each mean indicate statistically significant different means ($\alpha = 0.05$), as calculated with paired *t*-tests. The fourth row indicates the *p*-values from one-way ANOVA tests for significant differences in mean element quotas as a function of depth. Percent changes of C, N, and Si are means \pm (range $\div 2$ [$n = 2$]). Percent changes of S, P, Ni, Fe, and Zn are means \pm propagated SE ($n = 3$). Flux attenuation coefficients (*b'*) were calculated from non-linear fits of Martin's power law to SXRF data (see text for details) and are \pm SE. nd = not determined.

	C	N	S	P	Si	Ni	Fe	Zn
Cells in mixed-layer ($n=14$)	nd	nd	134 \pm 29a	51 \pm 8.2a	284 \pm 28a	17 \pm 5.3a	134 \pm 26a	343 \pm 60a
Cells in 100 m trap ($n=7$)	nd	nd	33 \pm 7.7b	23 \pm 7.6b	181 \pm 19a	3.8 \pm 1.3a	119 \pm 25a	132 \pm 27b
Cells in 200 m trap ($n=5$)	nd	nd	23 \pm 8.5b	17 \pm 3.7b	262 \pm 45a	6.9 \pm 2.3a	100 \pm 13a	84 \pm 15b
ANOVA <i>p</i> -value	nd	nd	0.011	0.026	0.146	0.175	0.724	0.013
Change in cell quotas from mixed-layer to 100 m trap (%)	nd	nd	75 \pm 24	55 \pm 20	36 \pm 5	78 \pm 36	11 \pm 3	61 \pm 16
Change in cell quotas from 100 m trap to 200 m trap (%)	nd	nd	32 \pm 14	28 \pm 11	-44 \pm 9	-81 \pm 39	16 \pm 4	37 \pm 10
Change in cell quotas from mixed-layer to 200 m trap (%)	nd	nd	83 \pm 36	67 \pm 18	8 \pm 2	61 \pm 27	25 \pm 6	76 \pm 19
Change in bulk element fluxes from 100 m trap to 200 m trap (%)	45 \pm 7	55 \pm 5	nd	66 \pm 18	85	42 \pm 38	4 \pm 2	66 \pm 31
Flux attenuation coefficient (<i>b'</i>)	nd	nd	1.09 \pm 0.60	0.63 \pm 0.28	0.12 \pm 0.11	0.90 \pm 0.76	0.13 \pm 0.17	0.77 \pm 0.34

Discussion

Analysis of trace metals Fe, Zn, and Ni in individual sinking diatom cells enables us to avoid operational definitions of biogenic vs. lithogenic material and focus unambiguously on sinking cellular material without the confounding influence of lithogenic particles that often hinders our understanding of trace element remineralization (Frew et al. 2006). Simultaneous bulk measurements of elements in sinking particles in the same traps allow us to make direct comparisons with traditional integrated fluxes. This dual approach reveals that these bioactive metals are lost from cells at different rates, likely via different mechanisms, with consequences for their geochemical fate.

Differential remineralization length scales—The data on cellular quotas and bulk elemental fluxes show that major elements associated with sinking phytoplankton are released at different rates and hence at different depths. Nearly two-thirds of cellular P and S were lost from the diatoms as they sank through the upper 200 m, while < 10% of cellular Si was lost. This dramatic difference in the lability of the major biomass elements in diatoms can be explained by the presence of Si in opal (SiO₂) frustules that are protected from immediate dissolution by an organic coating (Bidle and Azam 2001), while P and S (and N) are associated with organic biochemical moieties in the cells. Loss of Si from the cells requires prior degradation of the organic coating, while P- and S-containing molecules may be lost directly upon mechanical or microbial enzymatic attack to the cells. Further, bacterial respiration may create microenvironments of lowered pH that serve to enhance breakdown of organic molecules while stabilizing amorphous SiO₂, which is stable at lower pH (Alldredge and Cohen 1987). Careful leaching experiments with natural marine plankton assemblages have shown how readily P can be lost from cells (Collier and Edmond 1984), and the shallower depth of P remineralization compared with Si broadly matches vertical profiles of these nutrients in dissolved form and flux attenuation coefficients (calculated as the *b* coefficient with the Martin equation; Martin et al. 1987) measured in upper-water-column sediment traps in other regions (Table 5).

There is a discrepancy in the Si data, with the single-cell measurements showing insignificant loss from *A. glacialis* in contrast to the bulk flux data showing biogenic silica to be the most rapidly lost element (85% drop in Si flux between 100 m and 200 m). One explanation for this discrepancy may be different behavior of silica in sinking intact diatom cells compared with that of bulk detrital biogenic silica, which can comprise the majority of the biogenic Si (Krause et al. 2010). Silica detritus generated by zooplankton grazing and degraded by microbial enzymes can dissolve rapidly in under-saturated surface waters (Adjou et al. 2011), and roughly 50–75% of sinking biogenic silica can be solubilized in the upper water column (Treguer and De La Rocha 2013). In contrast, the intact diatom cells targeted with SXRF were clearly more resistant to dissolution, at least in the upper 200 m. Alternatively, the discrepancy may be caused by taxon-specific

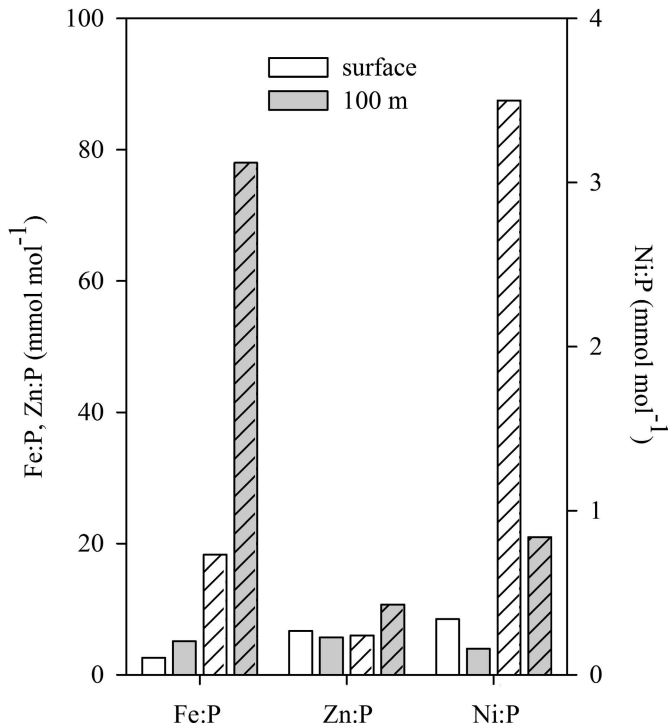


Fig 5. Phosphorus-normalized Fe, Zn, and Ni stoichiometries for individual cells (SXRF; solid bars) and bulk particulate material (ICPMS; hashed bars) collected from the surface mixed-layer (white bars) and the 100 m sediment trap (gray bars).

differences in dissolution or grazing of diatoms sinking through the water column. *A. glacialis* was the most abundant diatom in the surface mixed-layer at the time of sampling, but other diatom taxa were also present, including small centrics and pennates and larger chains of diatoms such as *Guinardia* spp. and *Leptocylindrus danicus* (data not shown). *A. glacialis* was well-represented in the trap material, but *Guinardia* spp. and *Leptocylindrus* spp. were not found in the traps (F. H. Chang pers. comm.), suggesting that these groups may have been more prone to

dissolution or grazing. There also may have been less intact *A. glacialis* cells present in the traps, but these were not chosen for SXRF analysis.

The cellular trace-metal constituents Fe, Ni, and Zn were also lost from cells at different rates, with Ni and Zn lost rapidly (likely in conjunction with P, S, and N) but Fe retained to a greater depth in the water column. As with the macronutrients, the bulk-trap flux data generally support the SXRF data, indicating a decoupling between the remineralization of Ni and Zn and retention—and potentially scavenging—of Fe. Comparisons of dissolved metal profiles also suggest that Fe is remineralized deeper than macronutrients N and P (Johnson et al. 1997; Frew et al. 2006), and dissolved profiles generally indicate that Ni and Zn are coupled to macronutrient remineralization (Bruland 1980). Ship-board incubations of natural plankton assemblages have also showed Ni to be more readily released than Fe (Collier and Edmond 1984).

There are few published data with which to directly compare these results. Lamborg et al. (2008) report Fe flux attenuation coefficients that may not be significantly different from 0 at Sta. ALOHA, and at Sta. K2 in the sub-arctic Northwest Pacific Fe fluxes increased with depth in the upper 500 m (Table 5). Zinc fluxes, when reported, showed little attenuation with depth. A long-term record of Fe fluxes to deeper sediment traps (> 500 m) in the Sargasso Sea also shows increasing Fe fluxes with depth (Conte et al. 2001). Such observations can be explained by lateral inputs of lithogenic and detrital particles, and scavenging of dissolved Fe may also contribute to particulate Fe fluxes. Such effects likely mask biological remineralization processes that are occurring in the water column, highlighting the limitations of bulk sediment-trap data for studying Fe remineralization.

Indeed, we observe bulk trace-metal fluxes that group according to broad geochemical classification (Kuss and Kremling 1999), potentially independent of elemental behavior in sinking cells. Bulk fluxes of Ni, Cu, Zn, and Cd attenuated at a rate similar to that of P, and Fe flux attenuated in step with Al and Ti (Fig. 7). The matching

Table 2. Element stoichiometries (mmol mol^{-1}) for *A. glacialis*, bulk material, and material remineralized from *A. glacialis* during trap deployment A2. Data for *A. glacialis* are mean stoichiometries of cells collected at 30 m ($n = 14$), 100 m ($n = 7$), and 200 m ($n = 5$). Data for the surface mixed-layer bulk-particle assemblage are from 30 m on day of the year 269. Blank spaces indicate values that were not calculated because of lack of consistent data across the depths. Dashes indicate negative values.

	Fe:P	Fe:S	Fe:Si	Zn:P	Zn:S	Zn:Si	Ni:P	Ni:S	Ni:Si
Surface mixed-layer									
<i>A. glacialis</i>	2.6	1.0	0.47	6.7	2.5	1.21	0.34	0.13	0.062
bulk particles	24	—	—	5.0	—	—	3.3	—	—
100 m trap									
<i>A. glacialis</i>	5.1	3.6	0.66	5.7	4.0	0.73	0.16	0.11	0.021
bulk particles	78	—	—	10.7	—	—	0.84	—	—
200 m trap									
<i>A. glacialis</i>	6.0	4.4	0.38	5.0	3.7	0.32	0.41	0.30	0.026
bulk particles	327	—	—	9.0	—	—	1.56	—	—
Remineralized material									
30–100 m	0.5	0.14	0.14	7.5	2.1	2.05	0.49	0.14	0.13
100–200 m	2.9	1.8	—	7.4	4.6	—	—	—	—

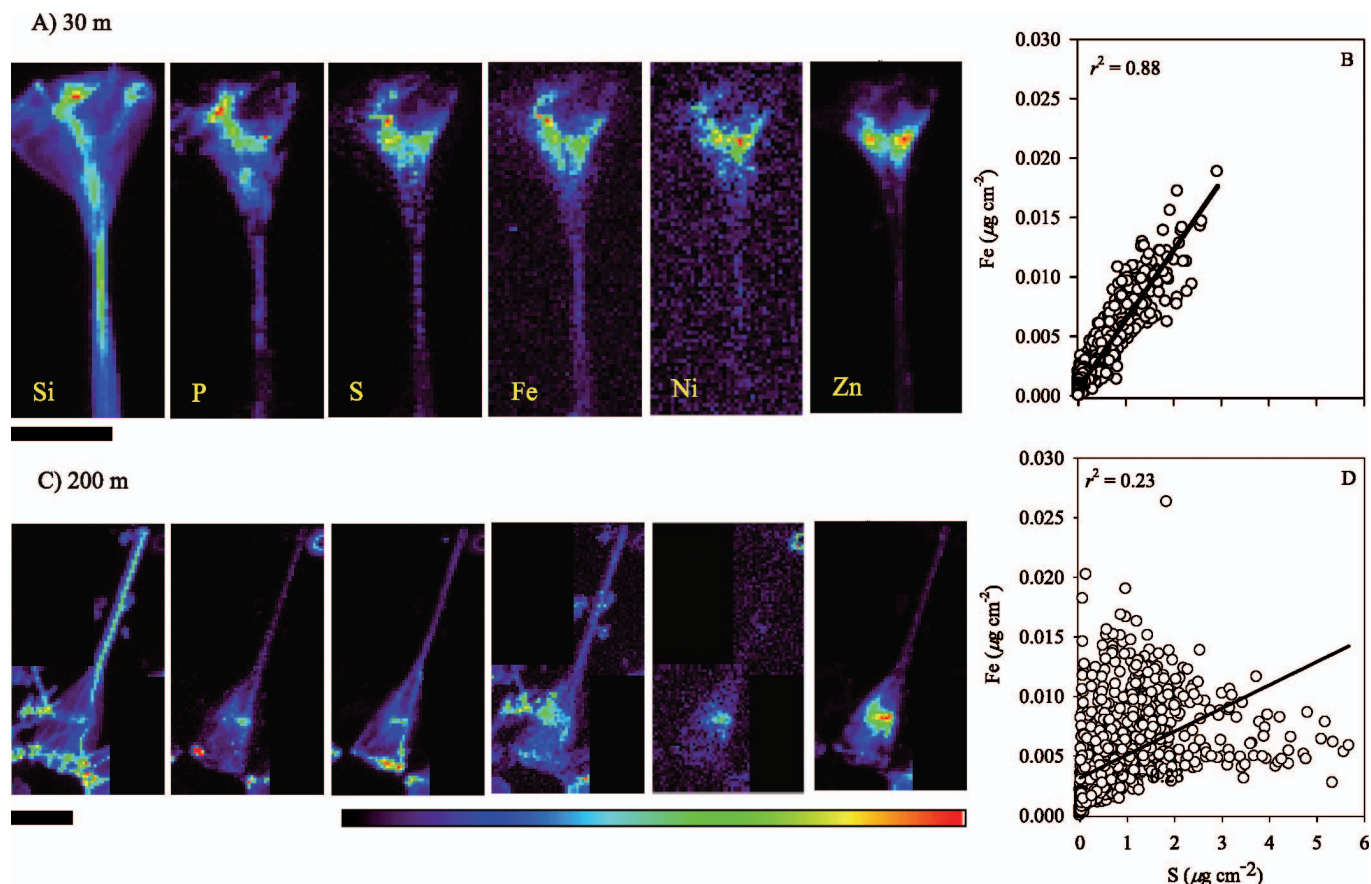


Fig. 6. False-color element maps (Si, P, S, Fe, Ni, Zn) and associated scatterplots of pixel-specific Fe and S concentrations for *Asterionellopsis glacialis* cells collected from (A, B) 30 m or (C, D) 200 m. Warmer colors indicate higher concentrations, but each map has a separate absolute scale. The scale bars indicate 10 μm for each cell. For the scatterplots, Fe and S concentrations for each pixel in the cell were extracted and plotted against each other. A linear regression has been fit to the data, and the resultant coefficient of determination (r^2) is shown on each plot.

Table 3. Mean (\pm SE) coefficients of determination and results of Kruskal–Wallis test for significance of depth effect. Eight, 7, and 5 samples were analyzed from the surface mixed-layer, 100 m, and 200 m, respectively. The number of samples from the surface mixed-layer was reduced by exclusion of cells analyzed during a synchrotron run in November 2009, when lower spatial resolution limited our ability to assess subcellular associations. Values reported for each of the three depths are means. The final column shows p -values for the test. p -values $<$ 0.05 indicate statistically significant changes in the spatial association of the two elements with depth.

	Surface	100 m	200 m	p -value
Fe–P	0.56 \pm 0.05	0.34 \pm 0.09	0.22 \pm 0.05	0.02
Fe–S	0.66 \pm 0.07	0.32 \pm 0.05	0.32 \pm 0.12	0.02
Fe–Si	0.31 \pm 0.03	0.19 \pm 0.04	0.27 \pm 0.05	0.20
Zn–P	0.48 \pm 0.08	0.15 \pm 0.06	0.27 \pm 0.08	0.03
Zn–S	0.67 \pm 0.09	0.50 \pm 0.07	0.48 \pm 0.15	0.27
Zn–Si	0.12 \pm 0.01	0.07 \pm 0.02	0.06 \pm 0.02	0.01
Ni–P	0.52 \pm 0.07	0.23 \pm 0.07	0.19 \pm 0.08	0.01
Ni–S	0.43 \pm 0.06	0.15 \pm 0.07	0.19 \pm 0.08	0.03
Ni–Si	0.21 \pm 0.06	0.14 \pm 0.06	0.04 \pm 0.08	0.02

behavior of Fe, Al, and Ti—despite significant differences in the concentrations of these metals in phytoplankton—indicates that Fe fluxes are dominated by lithogenic particles. This interpretation is supported by particulate Fe:P ratios that are $>$ 10-fold above those measured in cells (Table 2), and particulate Fe:Al ratios (0.21 ± 0.03 mol: mol across all trap samples) that are very close to crustal values in Australian dust samples (0.18 mol: mol; Frew et al. 2006). Lithogenic materials are significantly more resistant to microbial degradation (Boyd et al. 2010), so remineralization length-scales will likely vary as a function of the chemical composition of the sinking particles. Further, the proportions of lithogenic and biogenic particles will vary regionally (Boyd et al. 2010). By teasing apart such fundamental differences in the breakdown of biogenic and lithogenic particles, we can better constrain the biogeochemical roles of biogenic and lithogenic particles in setting the degree of coupling between minor and major elements in the ocean.

Mechanisms and sequence of remineralization—The light micrographs and single-cell analyses provide clues to the mechanisms by which elements are remineralized from sinking diatoms. If the cells had been grazed by mesozooplankton

Table 4. Wilcoxon Signed Rank Sum test for significant differences in spatial correlations within each depth classification. The values shown are p -values of the test for significant differences between pairs of elements within individual cells. Significant differences ($p < 0.05$) are shown in bold. In each case, comparisons are made between pairs of elements that share either a numerator or a denominator.

	Fe-P	Fe-S	Fe-Si	Zn-P	Zn-S	Zn-Si	Ni-P	Ni-S	Ni-Si
Surface cells ($n=8$)									
Fe-P	—	0.109	0.016	0.250			0.742		
Fe-S		—	0.023		0.844			0.023	
Fe-Si			—			0.008			0.250
Zn-P				—	0.008	0.008	1.000		
Zn-S					—	0.008		0.023	
Zn-Si						—			0.641
Ni-P							—	0.945	0.008
Ni-S								—	0.195
100 m cells ($n=7$)									
Fe-P	—	1.000	0.578	0.047			0.578		
Fe-S		—	0.047		0.078			0.078	
Fe-Si			—			0.078			0.375
Zn-P				—	0.016	0.156	0.813		
Zn-S					—	0.016		0.016	
Zn-Si						—			0.938
Ni-P							—	0.375	0.016
Ni-S								—	0.578
200 m cells ($n=5$)									
Fe-P	—	0.438	0.313	0.188			0.313		
Fe-S		—	0.438		0.125			0.188	
Fe-Si			—			0.063			0.063
Zn-P				—	0.125	0.063	0.188		
Zn-S					—	0.063		0.125	
Zn-Si						—			0.313
Ni-P							—	1.000	0.063
Ni-S								—	0.063

then they would have shown structurally compromised frustules and non-specific loss of elements. The presence of intact frustules and intracellular chlorophyll auto-fluorescence in the *A. glacialis* cells collected from 100 m and 200 m, as well as the diversity of elemental attenuation coefficients, indicate that cellular components were lost via autolysis or microbial activity rather than mechanical breakdown. The P- and S-normalized Zn and Ni stoichiometries in remineralized material were similar to these stoichiometries in whole cells in the upper water column, suggesting that Zn and Ni were remineralized as intact moieties, or at least in similar proportions to their presence in the cells. However, Fe : P and Fe : S stoichiometries

of remineralized material were only 15–20% of those in live cells, suggesting that Fe moieties were degraded. Alternatively, the presence of chlorophyll in the cells in the traps could indicate that Fe-rich photosystem proteins were preferentially retained by the cells.

Insight can be gained from a recent proteomic study that examined the proteome of the model centric diatom *Thalassiosira pseudonana* during a 28 d laboratory degradation experiment. Nunn et al. (2010) reported that the greatest loss of protein diversity occurred during the first 5 d of incubation after removal from light. Only one-third of proteins identified during mid-exponential growth could be detected after 5 d. In addition to microbial degradation,

Table 5. Summary of power law exponent (b) values for non-linear fits of Martin flux equation (Martin et al. 1987). *A. glacialis* data are from this study, and Lamborg data are for two stations in the Pacific Ocean (ALOHA and K2) and two separate sediment-trap deployments (1st and 2nd) at each station (Lamborg et al. 2008). nd = not determined. nr = not reported.

	S	P	Si	Ni	Fe	Zn
<i>Asterionellopsis glacialis</i>	1.09±0.60	0.63±0.28	0.12±0.11	0.90±0.76	0.13±0.17	0.77±0.34
Lamborg ALOHA – 1st	nd	0.88±0.48	0.65±0.22	nd	0.32±0.28	nr
Lamborg ALOHA – 2nd	nd	1.17±0.27	0.53±0.19	nd	0.22±0.26	nr
Lamborg K2 – 1st	nd	0.55±0.13	0.31±0.24	nd	–1.11±0.20	0.02±0.27
Lamborg K2 – 2nd	nd	0.97±0.12	0.20±0.12	nd	–0.46±0.27	0.14±0.16

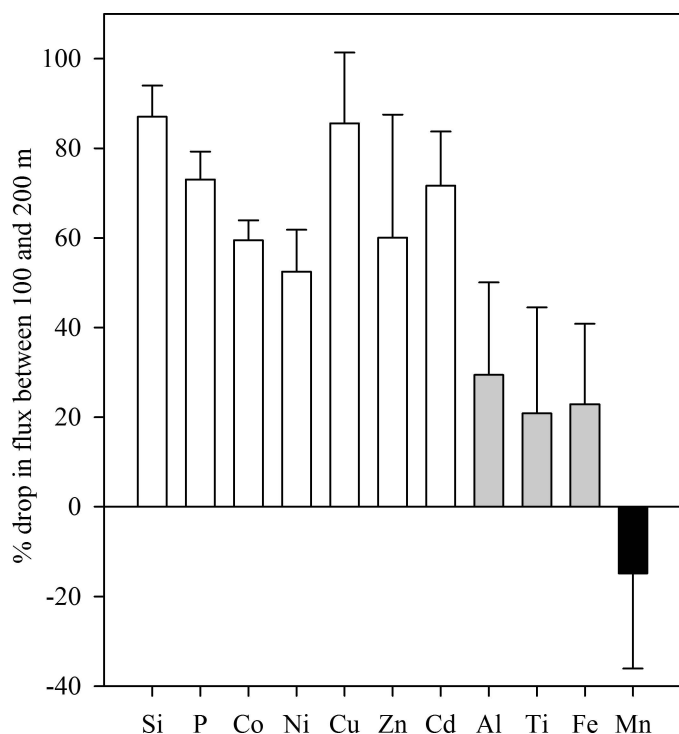


Fig. 7. Attenuation of bulk particulate element fluxes between 100 m and 200 m. Bars show mean (\pm standard deviation [SD]) percent decreases in element fluxes over three 72 h sediment-trap deployments (A2, A3, and A4) at 100 and 200 m. The elements are shaded according to their reported geochemical behavior. Fluxes of P, Co, Ni, Cu, Zn, and Cd are primarily associated with sinking biogenic material (white bars). Al, Ti, and Fe are likely dominated by lithogenic particles (gray bars). Mn fluxes increase slightly with depth, likely due to authigenic formation of Mn oxide particles or scavenging of Mn by particles (black bar).

diatoms also produce their own proteases under conditions of nutrient and light stress, which can enhance loss of cellular proteins (Berges and Falkowski 1998). During the 28 d incubation of Nunn et al. (2010), genomic DNA was degraded rapidly, while photosynthetic and related light-harvesting proteins were preferentially retained by the cells. After 23 d of microbial degradation, only four proteins could be identified: fucoxanthin chlorophyll *a,c*-binding protein 9, Fe transporter FTR1, proteophosphoglycan, and Clp-X proteinase (Nunn et al. 2010). The presence of these four proteins likely reflects their abundance during active cell growth, but also their protection within multiple membranes (typical of chloroplast-associated proteins) and association with lipid bilayers via multiple transmembrane domains. Other studies have found diatoms to retain photosynthetic proteins for prolonged periods of time (Peters and Thomas 1996), and photosynthetic competency can also be maintained in diatoms for up to 2 weeks (Berges and Falkowski 1998).

Spatial associations of Fe with biomass elements provide additional clues as to its fate during remineralization. Analysis of the distributions of elements within cells shows that Fe was less associated with Si than with P or S in live cells in the upper water column, but that Fe–Si co-localization did

not decrease as the cells sank. The close association between Fe and S suggests that Fe in live cells was associated primarily with proteins. As sinking cells were degraded, Fe proteins associated with the photosystems were likely preferentially retained relative to other proteins, explaining some of the decoupling. Additionally, as S (and protein) was lost from the cells, Fe was mostly retained (based on whole-cell quotas). The Fe could have been separated from the proteins within the cell, or the proteins degraded by extracellular proteases and the Fe re-scavenged to the frustule upon release. The spatial elemental analyses support the latter interpretation, matching the contention of Frew et al. (2006). A greater propensity of Fe to be scavenged by particles, relative to Zn and Ni, is supported by published field studies (Löscher 1999; Boyd and Ellwood 2010).

Analyses of quotas and spatial associations indicate that Zn had a different fate. Zn:S and Zn:P ratios of remineralized material matched that of the cells, and Zn and S showed a spatial association (mean $r^2 = 0.48$) even at 200 m, supporting stoichiometric evidence for biochemical Zn–protein coupling (Lee and Fisher 1993). Zinc-finger proteins associated with RNA and DNA transcription and repair are likely to be quantitatively the most abundant Zn proteins in the cells (Dupont et al. 2010), which helps explain the association of Zn and P, and SXRF analysis of healthy cells often shows Zn–P spatial associations (Twining et al. 2004). However Zn and S were significantly more co-located than Zn and P, and this difference was maintained at 100 m but lost by 200 m. Sulfur-containing cysteine moieties are directly bound to Zn in many of the Zn-finger proteins (Frausto Da Silva and Williams 2001). Zinc proteins likely remained somewhat intact at 100 m but became dissociated with their nuclear substrates.

Interestingly, there was no evidence for a (bio)chemical connection between Zn and Si in the sinking cells. The mean coefficient of determination for Zn and Si at 200 m ($r^2 = 0.06$) was the lowest of any element pair at any depth. This is in distinct contrast to previous bulk studies that have observed a connection between Zn and Si remineralization in the water column (Bruland 1980; Löscher 1999). This contradiction may be explained by different behavior of sinking intact diatoms vs. more detrital, grazer-damaged frustules. As noted above, significant remineralization of biogenic Si was observed in the bulk-trap data. The upper water column Si–Zn linkage noted in some regions may therefore be driven by dissolution of detrital diatom frustules or by the loss of Zn from sinking cells or aggregates combined with the loss of Si from detrital frustules. However, because only a few percent of cellular Zn in diatoms is associated with the frustule (Ellwood and Hunter 2000), the correlation of Zn and Si in the water column is likely also to be related to rates of diatom sinking and the simultaneous release of both elements from packaged sinking diatoms, for example in fecal pellets. An additional factor at play is the uptake of remineralized Zn—but not Si—by microbes working to degrade sinking diatoms, which might counteract the effects of decoupled release of the two elements from diatoms.

Nickel behavior was intermediate between Zn and Fe, both in terms of elemental loss rates and spatial associations. Nickel was lost almost as rapidly as Zn (similar to P), and like Zn Ni:P and Ni:S, remineralization ratios were similar to those in the cells. However, bulk Ni:P ratios in the traps were substantially higher than in cells, indicating the presence of an abiotic particulate fraction as well. The particulate Ni is probably not lithogenic material, because Ni content of upper continental crust is lower than Zn content (Wedepohl 1995), and Zn particulate stoichiometries were not elevated. However anthropogenic particles are more likely to be enriched in Ni relative to Zn (Desboeufs et al. 2005), and these may have been present in the particle assemblage. Nickel was associated somewhat more with P and S, and Ni was significantly more associated with P than with Si. Nickel was less associated with S than was Zn (Table 4), and this difference may be due to the secondary importance of S amino acids in urease and other Ni proteins as compared with their primary importance in Zn-finger proteins. Bulk studies have found a relationship between Ni remineralization and remineralization of both P and Si (Bruland 1980), and a recent SXRF study also found Ni to be associated with both elements in diatoms (Twining et al. 2012). However the current study found no spatial evidence for a Ni-Si association.

Vertical trends in sub-cellular spatial associations of elements suggest a defined sequence for biochemical degradation of diatoms. The tight coupling of Zn and S remineralization likely results from their common incorporation into Zn metalloproteins such as RNA and DNA polymerase and carbonic anhydrase (Frausto Da Silva and Williams 2001; Dupont et al. 2010). Therefore, these elements are probably lost simultaneously (along with P) during degradation of nucleic acids and related structures. Similarly, a fraction of cellular Ni may reside in phospholipid membranes, as is the case with other divalent transition metals (Horner et al. 2013). This could also result in the coupled bacterially mediated release of these elements from sinking cells in the upper 100 m. Although these elemental maps cannot directly demonstrate plasma membrane integrity or element associations with specific organelles, the degradation of internal features may only occur after external membranes have been broken down. In contrast to other elements, Fe and Si have much longer remineralization length-scales, but for different reasons. Silicon shows little dissolution until removal of the protective organic coating from the frustule (Bidle and Azam 1999), while Fe is lost but rapidly re-scavenged onto cells (Frew et al. 2006), suggesting that not all Fe is released from cells as unreactive organic complexes (Boyd et al. 2010).

Heterotrophic bacteria play a major role in the elemental recycling of sinking material, and therefore remineralization patterns may reflect both microbial demands for elemental building-blocks and the relative lability of structures, molecules and elements within sinking cells. Studies of bacterial enzymatic activity (Smith et al. 1992) and, recently, microbial genomics (Delong et al. 2006), reveal that major and minor elements are required to synthesize important enzymes. For example, Zn is needed for phosphatase and several extracellular proteases that are

used to remineralize specific compounds (Smith et al. 1992). Activities of aminopeptidase, phosphatase, and β -glucosidase, as well as leucine incorporation, were measured in trap particles and were elevated (on a volume-normalized basis) relative to water-column rates (data not shown). Bacteria were present and likely contributing to element remineralization.

The observed element remineralization trends could also have been caused by cellular autolysis. Cells may undergo this process after onset of nutrient limitation. Autolysis in diatoms has been observed to result in degradation of internal organelles, while cell membranes appeared to remain intact (Bidle and Bender 2008). Despite apparently intact membranes, some cells appeared empty after only a few days of degradation. Autolysis could explain loss of internal elements without loss of Si from the frustule. Pigment fluorescence also degrades during this process, but at a rate that would still allow the fluorescence observed in our trap-collected cells.

There are alternative—but not mutually exclusive—explanations for the observed remineralization trends. Trace-metal loss from sinking cells following microbial degradation or autolysis may be a function of solubility of the cellular components rather than specific biochemical pathways of degradation. Iron moieties such as those in photosystems and ferritin may be more resistant to dissolution than nucleic acids and hydrolyzed lipids and proteins. Observed trends may also be affected by potential localized complexation of metals. Cordero et al. (2012) concluded that bacteria attached to sinking particles can actively use Fe solubilized with siderophores, whether they synthesize the siderophores or not. Indeed, phytoplankton Fe that is solubilized by bacterial activity can be assimilated by attached bacteria in addition to Fe that is being scavenged. Both processes would serve to draw the Fe back in to the particulate pool, and we would not necessarily be able to tell them apart with the spatial and/or temporal resolution achieved here.

Implications—This study demonstrates that Fe is retained within sinking phytoplankton to a greater extent than macronutrients such as P and N. Stoichiometries of dissolved Fe, P, and N in the upper water column will thus not match the stoichiometries of these cellular components in sinking cells. Rather, dissolved Fe:N and Fe:P ratios, as well as ratios of Fe to apparent oxygen utilization, will underestimate Fe stoichiometries in phytoplankton. This is an important caveat, because this approach is used to estimate the Fe quotas of resident phytoplankton in open-ocean regions (Sunda 1997) and parameterize models (Moore et al. 2004). Although inter-ocean trends in phytoplankton Fe quotas may still be observed, care should be taken in extrapolating dissolved stoichiometries to cellular stoichiometries (Twining and Baines 2013). Oceanic phytoplankton likely contain more Fe than estimated from dissolved nutrient ratios. In contrast, cellular Zn and Ni quotas are probably accurately represented by dissolved nutrient data.

Biogenic transformations of sinking material in the water column have significant implications for global element cycling and climate (Kwon et al. 2009). However,

the mechanisms acting on sinking cells remain largely uncharacterized. Previous efforts to gain insight into these processes have applied primarily bulk geochemical (Martin et al. 1987; Lamborg et al. 2008) or, more recently, biological ‘-omics’ (Delong et al. 2006) techniques. It is no longer adequate merely to consider metal geochemistry as being affected by the behavior of metals associated with ‘soft parts’ and ‘hard parts.’ Clearly additional mechanisms are at play, which influence the resulting geochemical element distributions. Here, we have attempted to bridge these approaches through analysis of individual suspended and sinking cells, demonstrating the differential loss of elements from intact sinking cells consistent with microbial enzymatic activity. In this way, remineralization of each element may be driven by a combination of the location and lability of cellular components and the degree of microbial demand for particular elements. Our findings contribute to an improved mechanistic understanding of the biogeochemical roles played by specific organismal groups and classes of particles, as will be necessary to accurately model the stoichiometry and pathways of trace- and macro-nutrient resupply to the surface ocean.

Future advances may come from in-depth studies of microbial communities directly associated with sinking particles coupled to micro-analytical geochemical measurements. Combining genomic, transcriptomic, and proteomic information regarding microbial diversity and activity with elemental measurements of cell and particle composition should provide the mechanistic understanding of particle degradation needed to understand variations in the process across seasons (Lutz et al. 2007) and longer timescales over which climate conditions may change.

Acknowledgments

The FeCycle II project was supported by New Zealand Ministry of Science & Innovation funding to the Coasts and Oceans OBI program (PWB, SDN, EWM, CO1X0501) and by a grant from the U.S. National Science Foundation (OCE 0825379/0825405/0825319) to BST, SWW, and DAH. R. Frew, S. Searson, and L. Northcote assisted with sediment trap cleaning, deployment, and sample processing, respectively. F. Hoe Chang (National Institute of Water and Atmospheric Research) provided phytoplankton identification and counts. Use of the Advanced Photon Source, an Office of Science User Facility operated for the U.S. Department of Energy (DOE) Office of Science by Argonne National Laboratory, was supported by the U.S. DOE under Contract No. DE-AC02-06CH11357. We thank two anonymous reviewers for comments that improved the paper.

References

- ADJOU, M., P. TREGUER, C. DUMOUSSEAUD, R. CORVAISIER, M. A. BRZEZINSKI, AND D. M. NELSON. 2011. Particulate silica and Si recycling in the surface waters of the Eastern Equatorial Pacific. *Deep-Sea Res. Part II* **58**: 449–461, doi:10.1016/j.dsr2.2010.08.002
- ALLDREDGE, A. L., AND Y. COHEN. 1987. Can microscale patches persist in the sea? Microelectrode study of marine snow, fecal pellets. *Science* **235**: 689–691, doi:10.1126/science.235.4789.689
- BARRETT, P. M., J. A. RESING, N. J. BUCK, C. S. BUCK, W. M. LANDING, AND C. I. MEASURES. 2012. The trace element composition of suspended particulate matter in the upper 1000 m of the eastern North Atlantic Ocean: A16N. *Mar. Chem.* **142**: 41–53, doi:10.1016/j.marchem.2012.07.006
- BERGES, J. A., AND P. G. FALKOWSKI. 1998. Physiological stress and cell death in marine phytoplankton: Induction of proteases in response to nitrogen or light limitation. *Limnol. Oceanogr.* **43**: 129–135, doi:10.4319/lo.1998.43.1.0129
- BIDLE, K. D., AND F. AZAM. 1999. Accelerated dissolution of diatom silica by marine bacterial assemblages. *Nature* **397**: 508–512, doi:10.1038/17351
- , AND ———. 2001. Bacterial control of silicon regeneration from diatom detritus: Significance of bacterial ectohydrolases and species identity. *Limnol. Oceanogr.* **46**: 1606–1623, doi:10.4319/lo.2001.46.7.1606
- , AND S. J. BENDER. 2008. Iron starvation and culture age activate metacaspases and programmed cell death in the marine diatom *Thalassiosira pseudonana*. *Eukaryot. Cell* **7**: 223–236, doi:10.1128/EC.00296-07
- BOYD, P. W., AND M. J. ELLWOOD. 2010. The biogeochemical cycle of iron in the ocean. *Nature Geosci.* **3**: 675–682, doi:10.1038/ngeo964
- , E. IBISANMI, S. G. SANDER, K. A. HUNTER, AND G. A. JACKSON. 2010. Remineralization of upper ocean particles: Implications for iron biogeochemistry. *Limnol. Oceanogr.* **55**: 1271–1288, doi:10.4319/lo.2010.55.3.1271
- , AND OTHERS. 2012. Microbial control of diatom bloom dynamics in the open ocean. *Geophys. Res. Lett.* **39**: L18601.
- , AND T. W. TRULL. 2007. Understanding the export of biogenic particles in oceanic waters: Is there consensus? *Prog. Oceanogr.* **72**: 276–312, doi:10.1016/j.pcean.2006.10.007
- BRAGG, J. G., D. THOMAS, AND P. BAUDOUIN-CORNU. 2006. Variation among species in proteomic sulphur content is related to environmental conditions. *Proc. R. Soc. B* **273**: 1293–1300, doi:10.1098/rspb.2005.3441
- BREA, S., X. A. ALVAREZ-SALGADO, M. ALVAREZ, F. F. PEREZ, L. MEMERY, H. MERCIER, AND M. J. MESSIAS. 2004. Nutrient remineralization rates and ratios in the eastern South Atlantic. *J. Geophys. Res. - Oceans* **109**: C05030, doi:10.1029/2003JC00205
- BROECKER, W. S., AND T. H. PENG. 1982. *Tracers in the Sea*. Lamont-Doherty Geological Observatory Press.
- BRULAND, K. W. 1980. Oceanographic distributions of cadmium, zinc, nickel, and copper in the North Pacific. *Earth Planet Sci. Lett.* **47**: 176–198, doi:10.1016/0012-821X(80)90035-7
- CHESTER, R. 2003. *Marine geochemistry*, 2nd ed. Blackwell Publishing.
- COLLIER, R., AND J. EDMOND. 1984. The trace element geochemistry of marine biogenic particulate matter. *Prog. Oceanogr.* **13**: 113–199, doi:10.1016/0079-6611(84)90008-9
- CONTE, M. H., N. RALPH, AND E. H. ROSS. 2001. Seasonal and interannual variability in deep ocean particle fluxes at the Oceanic Flux Program (OFP)/Bermuda Atlantic Time Series (BATS) site in the western Sargasso Sea near Bermuda. *Deep-Sea Res. Part II* **48**: 1471–1505, doi:10.1016/S0967-0645(00)00150-8
- CORDERO, O. X., L. A. VENTOURAS, E. F. DELONG, AND M. F. POLZ. 2012. Public good dynamics drive evolution of iron acquisition strategies in natural bacterioplankton populations. *Proc. Natl. Acad. Sci. U. S. A.* **109**: 20059–20064, doi:10.1073/pnas.1213344109
- DELONG, E. F., AND OTHERS. 2006. Community genomics among stratified microbial assemblages in the ocean’s interior. *Science* **311**: 496–503, doi:10.1126/science.1120250
- DESBOEUF, K. V., A. SOFIKITIS, R. LOSNO, J. L. COLIN, AND P. AUSSET. 2005. Dissolution and solubility of trace metals from natural and anthropogenic aerosol particulate matter. *Chemosphere* **58**: 195–203, doi:10.1016/j.chemosphere.2004.02.025
- DOWNES, M. T. 1978. An improved hydrazine reduction method for the automated determination of low nitrate levels in freshwater. *Water Res.* **12**: 673–675, doi:10.1016/0043-1354(78)90177-X

- DUPONT, C. L., A. BUTCHER, R. E. VALAS, P. E. BOURNE, AND G. CAETANO-ANOLLES. 2010. History of biological metal utilization inferred through phylogenomic analysis of protein structures. *Proc. Natl. Acad. Sci. U. S. A.* **107**: 10567–10572, doi:10.1073/pnas.0912491107
- EGGIMANN, D. W., AND P. R. BETZER. 1976. Decomposition and analysis of refractory oceanic suspended materials. *Anal. Chem.* **48**: 886–890, doi:10.1021/ac60370a005
- ELLWOOD, M. J., AND K. A. HUNTER. 2000. The incorporation of zinc and iron into the frustule of the marine diatom *Thalassiosira pseudonana*. *Limnol. Oceanogr.* **45**: 1517–1524, doi:10.4319/lo.2000.45.7.1517
- FRAUSTO DA SILVA, J. R. R., AND R. J. P. WILLIAMS. 2001. The biological chemistry of the elements: The inorganic chemistry of life, 2nd ed. Oxford Univ. Press.
- FREW, R. D., AND OTHERS. 2006. Particulate iron dynamics during FeCycle in subAntarctic waters southeast of New Zealand. *Glob. Biogeochem. Cycles* **20**: GB1S93, doi:10.1029/2005GB002558
- HAMADY, M., J. J. WALKER, J. K. HARRIS, N. J. GOLD, AND R. KNIGHT. 2008. Error-correcting barcoded primers for pyrosequencing hundreds of samples in multiplex. *Nat. Meth.* **5**: 235–237, doi:10.1038/nmeth.1184
- HORNER, T. J., R. B. Y. LEE, G. M. HENDERSON, AND R. E. M. RICKABY. 2013. Nonspecific uptake and homeostasis drive the oceanic cadmium cycle. *Proc. Natl. Acad. Sci. U. S. A.* **110**: 2500–2505, doi:10.1073/pnas.1213857110
- JOHNSON, K. S., R. M. GORDON, AND K. H. COALE. 1997. What controls dissolved iron concentrations in the world ocean? *Mar. Chem.* **57**: 137–161, doi:10.1016/S0304-4203(97)00043-1
- KARL, D. M., G. A. KNAUER, AND J. H. MARTIN. 1988. Downward flux of particulate organic matter in the ocean: A particle decomposition paradox. *Nature* **332**: 438–441, doi:10.1038/332438a0
- KING, A. L., AND OTHERS. 2012. A comparison of biogenic iron quotas during a diatom spring bloom using multiple approaches. *Biogeosciences* **9**: 667–687, doi:10.5194/bg-9-667-2012
- KRAUSE, J. W., AND OTHERS. 2010. The effects of biogenic silica detritus, zooplankton grazing, and diatom size structure on silicon cycling in the euphotic zone of the eastern equatorial Pacific. *Limnol. Oceanogr.* **55**: 2608–2611, doi:10.4319/lo.2010.55.6.2608
- KUSS, J., AND K. KREMLING. 1999. Particulate trace element fluxes in the deep northeast Atlantic Ocean. *Deep-Sea Res. Part I* **46**: 149–169.
- KWON, E. Y., F. PRIMEAU, AND J. L. SARMIENTO. 2009. The impact of remineralization depth on the air-sea carbon balance. *Nat. Geosci.* **2**: 630–635, doi:10.1038/ngeo612
- LAMBORG, C. H., K. O. BUESSELER, AND P. J. LAM. 2008. Sinking fluxes of minor and trace elements in the North Pacific Ocean measured during the VERTIGO program. *Deep-Sea Res. Part II* **55**: 1564–1577, doi:10.1016/j.dsr2.2008.04.012
- LEE, B.-G., AND N. S. FISHER. 1992. Degradation and elemental release rates from phytoplankton debris and their geochemical implications. *Limnol. Oceanogr.* **37**: 1345–1360, doi:10.4319/lo.1992.37.7.1345
- , AND ———. 1993. Release rates of trace elements and protein from decomposing planktonic debris. 1. Phytoplankton debris. *J. Mar. Res.* **51**: 391–421, doi:10.1357/0022240933223774
- LOH, A. N., AND J. E. BAUER. 2000. Distribution, partitioning and fluxes of dissolved and particulate organic C, N and P in the eastern North Pacific and Southern Oceans. *Deep-Sea Res. Part I* **47**: 2287–2316.
- LÖSCHER, B. M. 1999. Relationships among Ni, Cu, Zn, and major nutrients in the Southern Ocean. *Mar. Chem.* **67**: 67–102, doi:10.1016/S0304-4203(99)00050-X
- LUTZ, M. J., K. CALDIERA, R. B. DUNBAR, AND M. J. BEHRENFELD. 2007. Seasonal rhythms of net primary production and particulate organic carbon flux describe biological pump efficiency in the global ocean. *J. Geophys. Res.* **112**: C10011, doi:10.1029/2006JC003706
- MARTIN, J. H., G. A. KNAUER, D. M. KARL, AND W. W. BROENKOW. 1987. VERTEX: Carbon cycling in the northeast Pacific. *Deep-Sea Res.* **34**: 267–285.
- MOORE, J. K., S. C. DONEY, AND K. LINDSAY. 2004. Upper ocean ecosystem dynamics and iron cycling in a global three-dimensional model. *Glob. Biogeochem. Cycles* **18**: GB4028, doi:10.1029/2004GB002220
- NOBLE, A. E., AND OTHERS. 2012. Basin-scale inputs of cobalt, iron, and manganese from the Benguela–Angola front to the South Atlantic Ocean. *Limnol. Oceanogr.* **57**: 989–1010, doi:10.4319/lo.2012.57.4.0989
- NUNN, B. L., Y. S. TING, L. MALMSTROM, Y. S. TSAI, A. SQUIER, D. R. GOODLETT, AND H. R. HARVEY. 2010. The path to preservation: Using proteomics to decipher the fate of diatom proteins during microbial degradation. *Limnol. Oceanogr.* **55**: 1790–1804, doi:10.4319/lo.2010.55.4.1790
- PETERS, E., AND D. N. THOMAS. 1996. Prolonged darkness and diatom mortality I: Marine Antarctic species. *J. Exp. Mar. Biol. Ecol.* **207**: 25–41, doi:10.1016/S0022-0981(96)02520-8
- RAGUENEAU, O., AND P. TRÉGUER. 1994. Determination of biogenic silica in coastal waters: Applicability and limits of the alkaline digestion method. *Mar. Chem.* **45**: 43–51, doi:10.1016/0304-4203(94)90090-6
- SCHNEIDER, B., R. SCHLITZER, G. FISCHER, AND E. M. NOTHIG. 2003. Depth-dependent elemental compositions of particulate organic matter (POM) in the ocean. *Glob. Biogeochem. Cycles* **17**: no. 2, 1032, doi:10.1029/2002GB001871
- SHAFFER, G., J. U. BENDTSEN, AND O. ULLOA. 1999. Fractionation during remineralization of organic matter in the ocean. *Deep-Sea Res. Part I* **46**: 185–204.
- SMITH, D. C., M. SIMON, A. L. ALLDREDGE, AND F. AZAM. 1992. Intense hydrolytic enzyme activity on marine aggregates and implications for rapid particle dissolution. *Nature* **359**: 139–142, doi:10.1038/359139a0
- STEINBERG, D. K., B. A. S. VAN MOOY, K. O. BUESSELER, P. W. BOYD, T. KOBARI, AND D. M. KARL. 2008. Bacterial vs. zooplankton control of sinking particle flux in the ocean's twilight zone. *Limnol. Oceanogr.* **53**: 1327–1338, doi:10.4319/lo.2008.53.4.1327
- STERNER, R. W., AND J. J. ELSER. 2002. Ecological stoichiometry. Princeton Univ. Press.
- SUNDA, W. G. 1997. Control of dissolved iron concentrations in the world ocean: A comment. *Mar. Chem.* **57**: 169–172, doi:10.1016/S0304-4203(97)00045-5
- TANG, D. G., AND F. M. M. MOREL. 2006. Distinguishing between cellular and Fe-oxide-associated trace elements in phytoplankton. *Mar. Chem.* **98**: 18–30, doi:10.1016/j.marchem.2005.06.003
- TOVAR-SANCHEZ, A., S. A. SANUDO-WILHELMY, M. GARCIA-VARGAS, R. S. WEAVER, L. C. POPELS, AND D. A. HUTCHINS. 2003. A trace metal clean reagent to remove surface-bound iron from marine phytoplankton. *Mar. Chem.* **82**: 91–99, doi:10.1016/S0304-4203(03)00054-9
- TREGUER, P. J., AND C. L. DE LA ROCHA. 2013. The world ocean silica cycle. *Annu. Rev. Mar. Sci.* **5**: 477–501, doi:10.1146/annurev-marine-121211-172346
- TWINING, B. S., AND S. B. BAINES. 2013. The trace metal composition of marine phytoplankton. *Annu. Rev. Mar. Sci.* **5**: 191–215, doi:10.1146/annurev-marine-121211-172322

- , ———, J. B. BOZARD, S. VOGT, E. A. WALKER, AND D. M. NELSON. 2011. Metal quotas of plankton in the equatorial Pacific Ocean. *Deep-Sea Res. Part II* **58**: 325–341, doi:10.1016/j.dsr2.2010.08.018
- , ———, N. S. FISHER, AND M. R. LANDRY. 2004. Cellular iron contents of plankton during the Southern Ocean Iron Experiment (SOFeX). *Deep-Sea Res. Part I* **51**: 1827–1850.
- , AND OTHERS. 2003. Quantifying trace elements in individual aquatic protist cells with a synchrotron x-ray fluorescence microprobe. *Anal. Chem.* **75**: 3806–3816, doi:10.1021/ac034227z
- , ———, S. VOGT, AND D. M. NELSON. 2012. Role of diatoms in nickel biogeochemistry in the ocean. *Glob. Biogeochem. Cycles* **26**: GB4001, doi:10.1029/2011GB004233
- WANG, Y., AND P. Y. QIAN. 2009. Conservative fragments in bacterial 16S rRNA genes and primer design for 16S ribosomal DNA amplicons in metagenomic studies. *PLoS One* **4**: e7401, doi:10.1371/journal.pone.0007401
- WEDEPOHL, K. H. 1995. The composition of continental crust. *Geochim. Cosmochim. Acta* **59**: 1217–1232, doi:10.1016/0016-7037(95)00038-2
- WELLER, D. I., AND OTHERS. 2013. Temporal variation of dissolved methane in a subtropical mesoscale eddy during a phytoplankton bloom in the southwest Pacific Ocean. *Prog. Oceanogr.* **116**: 193–206, doi:10.1016/j.pocean.2013.07.008
- WELSCHMEYER, N. A. 1994. Fluorometric analysis of chlorophyll *a* in the presence of chlorophyll *b* and pheopigments. *Limnol. Oceanogr.* **39**: 1985–1992, doi:10.4319/lo.1994.39.8.1985

Associate editor: Mary I. Scranton

Received: 22 June 2013
Accepted: 01 January 2014
Amended: 03 January 2014